Topographic Mapping from the Retina to the Midbrain Is Controlled by Relative but Not Absolute Levels of EphA Receptor Signaling

Arthur Brown,[1,7,8] Paul A. Yates[1,4,7] Patrick Burrola,[1]
Dan Ortuño,[1] Ashish Vaidya,[3] Thomas M. Jessell,[5]
Samuel L. Pfaff,[2] Dennis D. M. O'Leary,[1]
and Greg Lemke[1,6]
[1] Molecular Neurobiology Laboratory
[2] Gene Expression Laboratory
The Salk Institute
La Jolla, California 92037
[3] John P. Robarts Research Institute and
Department of Physiology
University of Western Ontario
London, Ontario N6A 5K8
Canada
[4] Department of Neurosciences
University of California, San Diego
La Jolla, California 92093
[5] Howard Hughes Medical Institute
Department of Biochemistry and Molecular Biophysics
Columbia University
New York, New York 10032

Summary

Topographic maps are a fundamental feature of sensory representations in nervous systems. The formation of one such map, defined by the connection of ganglion cells in the retina to their targets in the superior colliculus of the midbrain, is thought to depend upon an interaction between complementary gradients of retinal EphA receptors and collicular ephrin-A ligands. We have tested this hypothesis by using gene targeting to elevate EphA receptor expression in a subset of mouse ganglion cells, thereby producing two intermingled ganglion cell populations that express distinct EphA receptor gradients. We find that these two populations form separate maps in the colliculus, which can be predicted as a function of the net EphA receptor level that a given ganglion cell expresses relative to its neighbors.

Introduction

Multicellular organisms require precise neural representations of their surroundings in order to respond appropriately to external stimuli and challenges (Kaas, 1997). In vertebrates, the projection of the retinal ganglion cells (RGCs) of the eye to their synaptic targets in the superior colliculus (SC) of the midbrain has served as an informative model system for understanding how such representations are formed (Fraser and Hunt, 1980; Goodhill and Richards, 1999; O'Leary et al., 1999). This projection is organized into a topographic map, in which, to a first

[6] To whom correspondence should be addressed (e-mail: lemke@salk.edu).
[7] These authors contributed equally to this work.
[8] Present address: John P. Robarts Research Institute and Department of Physiology, University of Western Ontario, London, Ontario N6A 5K8, Canada.

approximation, the Cartesian coordinates of a two-dimensional sheet of RGCs are mapped onto a second two-dimensional sheet of target neurons in the SC. Thus, RGC axons from the extreme nasal retina project to the caudal (posterior) end of the SC (referred to as the tectum in nonmammalian vertebrates), whereas RGCs in the extreme temporal retina project to the rostral (anterior) end; RGCs located at intermediate temporal-nasal (t-n) retinal positions project to correspondingly intermediate positions along the rostral-caudal (r-c) axis of the SC. The dorsal-ventral axis of the retina, orthogonal to the t-n axis, is similarly mapped onto the lateral-medial axis of the SC.

The chemoaffinity hypothesis (Sperry, 1963) has been the favored model for how the retinocollicular map is formed. This hypothesis posits that the specificity of topographic projections is determined by interacting molecular "tags," which are distributed in complementary gradients on both projecting axons and their targets (Sperry, 1963). In vitro assays suggest that in the retinocollicular system, the graded tags envisioned by Sperry take the form of a cell surface, glycosyl phosphatidylinositol (GPI)-linked axon-repellent activity, distributed in a low-rostral-to-high-caudal gradient in the SC (Cox et al., 1990; Stahl et al., 1990); and one or more receptors for this activity, expressed in a low-nasal-to-high-temporal gradient by RGCs and their axons (Baier and Bonhoeffer, 1992).

Recent studies have implicated members of the Eph family of receptor protein-tyrosine kinases (PTKs), together with their ephrin ligands, as these graded molecular tags (for reviews, see Flanagan and Vanderhaeghen, 1998; O'Leary and Wilkinson, 1999; O'Leary et al., 1999). The large Eph family is divided into two subfamilies—EphA (A1–A8) and EphB (B1–B6), and the eight ephrin ligands are similarly divided into A (A1–A5) and B (B1–B3) subsets; ephrin-As are anchored by a GPI linkage, and ephrin-Bs by a transmembrane domain (Eph Nomenclature Committee, 1997). With few exceptions, ephrin-As bind and activate all of the EphA receptors, albeit with different affinities; and the same is true for the ephrin-Bs and their EphB receptors. Only limited interaction has been observed between the subfamilies (Orioli and Klein, 1997).

Ephrin-A2 and -A5 in combination generate a low-rostral-to-high-caudal gradient in the chick tectum (Cheng et al., 1995; Drescher et al., 1995); and EphA3, a preferred receptor for ephrin-A2 and -A5, exhibits a low-nasal-to-high-temporal distribution in the RGCs of the chick retina (Cheng et al., 1995). Thus, nasal RGCs, which have the lowest levels of EphA3, project to caudal tectum, where the levels of ephrin-A2/A5 are highest; and conversely, temporal RGCs, which have the highest levels of EphA3, project to rostral tectum, where ephrin-As are lowest. Consistent with these relationships, in vitro analyses using membrane stripe and growth cone collapse assays, together with ephrin-A2 misexpression studies in the developing chick tectum, support the hypothesis that ephrin-A2 and -A5 act as repellents for RGC axons, most strongly for those that originate in the

temporal retina (Nakamoto et al., 1996; Monschau et al., 1997). Similarly, the aberrant retinocollicular projections seen in mice with a deletion of the *ephrin-A5* gene (Frisén et al., 1998) suggest that ephrin-A2 and -A5 together form a smooth gradient of ephrin expression and axon-repellent activity across the mouse SC (Zhang et al., 1996; Frisén et al., 1998); and when both of these collicular ligands are eliminated entirely, most features of retinocollicular r-c topography are lost (Feldheim et al., 2000).

The action of the ephrin-A ligands in mediating the development of r-c order in the retinocollicular projection is assumed to be due to their activation of the EphA receptors expressed on RGC axons. More importantly, it is further assumed that the differential responses of RGC axons along the t-n axis of the retina are due to graded, position-dependent differences in the expression level of EphA receptors. To date, these fundamental assumptions have not been tested. Nor has the importance of EphA signaling relative to other hypothesized mechanisms for retinal axon guidance—such as correlated electrical activity (Yen et al., 1995; Zhang et al., 1998), differential cell adhesion (Bastmeyer et al., 1995; Miskevich et al., 1998), or RGC competition—been assessed.

We have performed a set of genetic manipulations in the mouse that test these assumptions. In contrast to the chick, EphA3 is not expressed by mouse RGCs (Feldheim et al., 1998). Instead, the closely related receptors EphA5 and EphA6 are both expressed in a low-nasal-to-high-temporal RGC gradient (see below). Although a compound knockout of both the mouse *EphA5* and *EphA6* genes might in theory be useful, this manipulation would eliminate the retinal receptor gradient entirely, and thus provide only a qualitative test of what is a quantitative model; moreover, the embryonic lethality of *EphA6* single knockouts alone (N. Gale and G. D. Yancopoulos, personal communication) precludes this approach in the absence of conditional gene inactivation. We have therefore adopted a gain-of-function strategy, and generated "knockin" mice in which an *IRES-EphA3* cDNA cassette is inserted into the 3′ untranslated region of the LIM homeobox gene *Islet2* (*Isl2*) (Tsuchida et al., 1994). *Isl2* is expressed in ~50% of RGCs, evenly distributed across the t-n axis of the retina (see below). The use of the *Isl2* gene to drive ectopic EphA3 expression is predicted to produce two interspersed populations of RGCs: one with the aggregate wild-type level of EphA receptors (EphA5 + A6), and a second in which the expression of EphA3 is superimposed upon this wild-type level.

If graded expression of retinal EphA receptors is sufficient for chemoaffinity-based mapping, several predictions with respect to the retinocollicular projection of such mixed sets of RGCs should be fulfilled. First, for any given retinal locus in the knockins, axons arising from RGCs expressing *Isl2/EphA3* (the $Isl2^+$ neurons) should project to a collicular position rostral to the projection arising from adjacent EphA3-RGCs, thus giving rise to two termination zones (TZs) in the SC, rather than the single zone seen in wild-type. Second, the degree of r-c separation of the two TZs should be a function of gene dosage: $Isl2^-$ *EphA3* homozygotes should exhibit greater separation than heterozygotes. Third, this separation might be expected to be less pronounced in projections arising from the temporal retina, since the relative difference in summed EphA receptor levels between $Isl2^+$ and $Isl2^-$ RGCs should decrease as the endogenous EphA5 + A6 level rises; and this temporal "narrowing" should be more pronounced in *Isl2-EphA3* heterozygotes than in homozygotes. We describe the results obtained from tests of each of these predictions, which together demonstrate that retinocollicular mapping is independent of the absolute level of EphA receptor signaling in RGCs, but at the same time is strongly dependent on relative differences in EphA signaling that exist between neighboring RGCs.

Results

Isl2-Based Targeting of EphA3 to Retinal Ganglion Cells

Our targeting strategy is based on the expression profiles of EphA receptors and Isl2 in the retina during the first two postnatal weeks, the period in which the murine retinocollicular map is established and refined (Simon et al., 1992; Frisén et al., 1998). As illustrated in Figure 1A, *EphA3* mRNA is present in the newborn mouse retina in the developing inner nuclear and presumptive photoreceptor layers, but not in the RGCs. Instead, the two EphA receptors that are expressed in RGCs and are appropriately graded along the retinal t-n axis are EphA5 and EphA6 (Figures 1B and 1C; Feldheim et al., 1998, 2000). EphA4 is also expressed in the developing mouse RGC layer, but as in the chick (Monschau et al., 1997; Connor et al., 1998), its expression is not graded (data not shown). *Isl2* mRNA is expressed in small clusters of RGCs, evenly scattered across the retinal t-n axis (Figure 1D). We estimate that ~50% of RGCs at postnatal day 12 are $Isl2^+$, since ~20% of the cells in the RGC layer express *Isl2* (Figure 2D), and since displaced amacrine cells account for ~60% of the cells in this layer (Jeon et al., 1998).

Given these expression profiles, we built the targeting construct diagrammed in Figure 2A. A full-length mouse *EphA3* cDNA, flanked at the 5′ end by an internal ribosome entry site (IRES) and at the 3′ end by a polyadenylation signal, was inserted into the mouse *Isl2* gene, at an SphI site in DNA encoding the 3′ untranslated region of the *Isl2* mRNA (Figure 2A; see Experimental Procedures). Since no *Isl2* DNA is deleted in this construct, all of the regulatory elements that normally control the cellular specificity of *Isl2* expression remain in place upon recombination of the construct into the *Isl2* locus. Preliminary experiments in which an IRES-flanked tau-lacZ expression cassette was inserted into the same position as the *EphA3* cDNA, and then knocked into the mouse *Isl2* locus, demonstrated selective tau-lacZ expression in cell populations previously shown to be $Isl2^+$ (data not shown).

The knockin strategy illustrated in Figure 2 affords a number of advantages. First, since mouse RGCs do not normally express *EphA3*, its expression in the knockin retina can easily be monitored, despite the expression of endogenous EphA5/A6. Given that the ephrin-As expressed in the mouse SC, (a) have been reported to
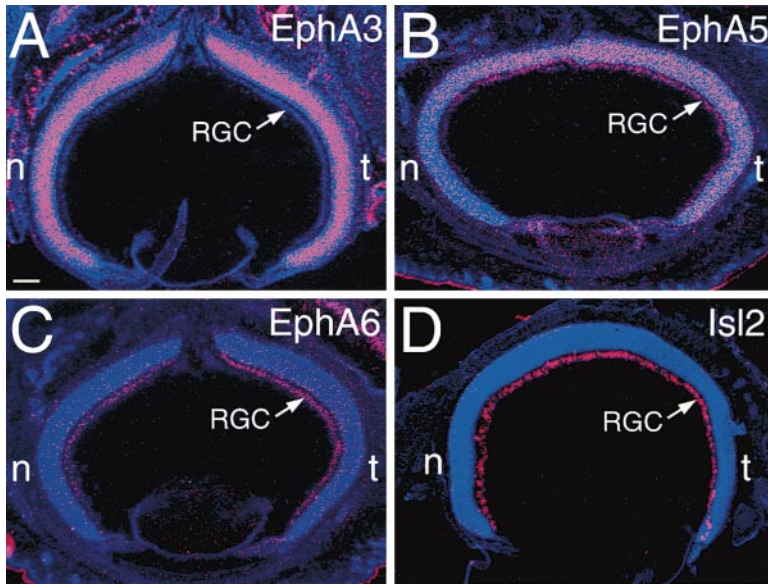
Figure 1. Expression of mRNAs Encoding EphA Receptors and *Isl2* in the Mouse Retina

^{35}S-RNA in situ hybridization signals for the *EphA3* (A), *EphA5* (B), *EphA6* (C), and *Isl2* (D) mRNAs on the day of birth (P0) in the mouse retina. *EphA3* is highly expressed in the mouse retina, but not in the retinal ganglion cell (RGC) neurons. *EphA5* and *EphA6* are both expressed by RGCs in a graded fashion, with low levels at the nasal side of the retina (n) and high levels at the temporal side (t). *Isl2* is expressed in ~50% of RGC neurons, in patches that are distributed evenly across the t-n axis of the retina. Higher power views of the *Isl2* expression pattern, as refined from P0 to P12, are illustrated in Figures 2C and 2D. Scale bar = 100 μm.

bind EphA3 and A5 with similar affinities (Cheng and Flanagan, 1994; Gale et al., 1996; Flanagan and Vanderhaeghen, 1998), and (b) interchangeably induce autophosphorylation of these receptors and EphA6 in cells in vitro (Davis et al., 1994; Gale et al., 1996; Flanagan and Vanderhaeghen, 1998), an axon's response should reflect the summed contribution of its complement of EphA receptors (Gale et al., 1996; Monschau et al., 1997).
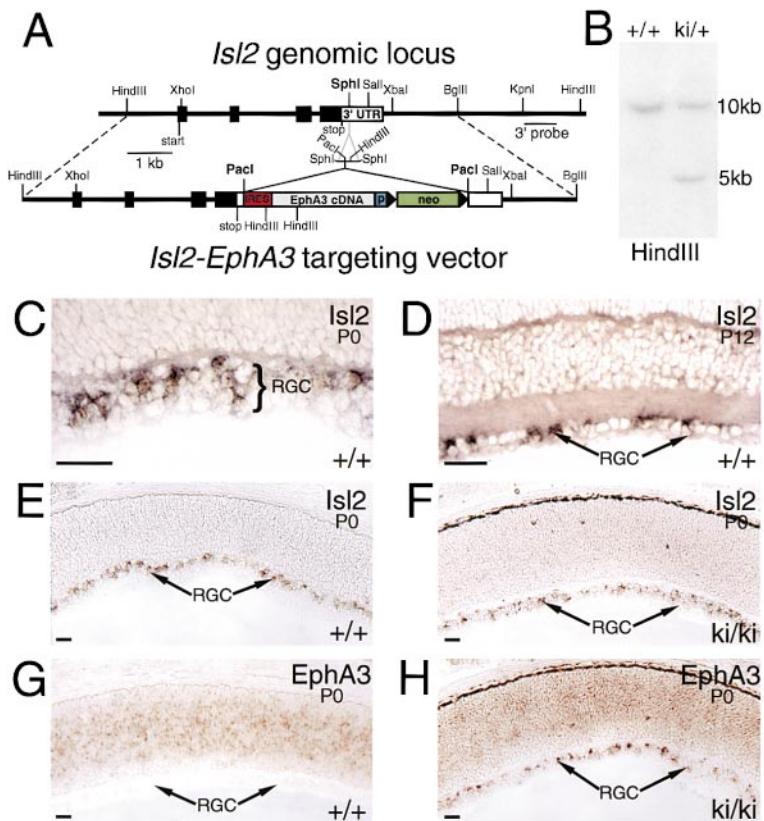

Figure 2. Structure of the *Isl2-EphA3* Targeting Allele and Its Expression in Knockin Mice

(A) The structure of the mouse *Isl2* locus is diagrammed above, and that of the *Isl2-EphA3* targeting vector below. See Experimental Procedures for details. Selected restriction sites are indicated. Black and white boxes denote coding and untranslated sequence, respectively. The external 3' probe used for Southern blot assessment of homologous recombination of the targeting vector into the *Isl2* locus is indicated.

(B) Southern blot of HindIII-digested DNA from a wild-type mouse (+/+) and from a mouse heterozygous for homologous recombination of the knockin allele (ki/+). The 5 kb band detected in the ki/+ lane runs from a HindIII site in the short polylinker used for cloning the IRES-EphA3-neo cassette to a HindIII site downstream of the 3' BglII end of the targeting vector.

(C) High power view of *Isl2* expression (dark signal; digoxygenin-labeled probe) in a subset of cells in the retinal ganglion cell (RGC) layer at postnatal day 0 (P0) in wild-type (+/+) mice.

(D) High power view of *Isl2* expression in ~20% of cells in the more fully developed RGC layer (arrowed) at postnatal day 12 (P12) in wild-type (+/+) mice. The murine retinocollicular projection is fully refined by the end of the second postnatal week; all anterograde and retrograde tracing studies were performed from P11 to P16.

(E) Low power view of *Isl2* expression in a subset of cells in the wild-type (+/+) P0 RGC layer (arrowed).

(F) Mosaic *Isl2* expression in RGCs is maintained in *Isl2-EphA3* homozygous (ki/ki) mice.

(G) *EphA3* mRNA is expressed in the inner layers of the wild-type mouse (+/+) P0 retina, but not in the RGC layer.

(H) Ectopic *EphA3* mRNA appears in a mosaic pattern, identical to that of *Isl2*, in a subset of P0 RGCs in *Isl2-EphA3* homozygous (ki/ki) mice. All scale bars = 50 μm.
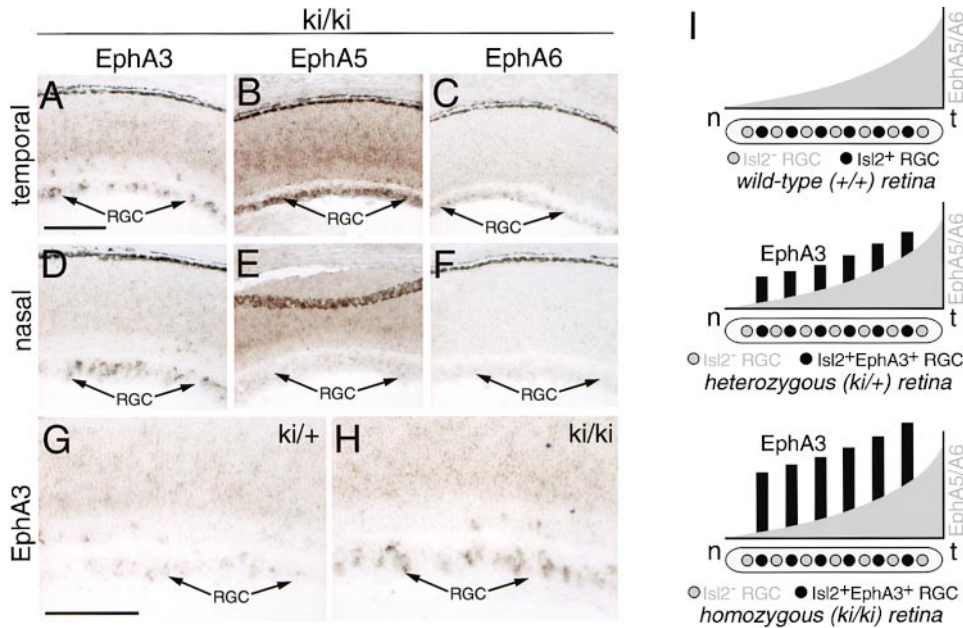
Figure 3. EphA Receptor Expression Profiles in Knockin Mice

Adjacent sections from the temporal (A–C) and nasal (D–F) retina of *Isl2-EphA3* homozygotes (ki/ki) were hybridized in situ, on the same slides, with identical-length digoxygenin-labeled probes for the *EphA3* (A and D), *EphA5*, (B and E), and *EphA6* (C and F) mRNAs. The retinal ganglion cell (RGC) layer in each section is arrowed. In situ hybridization of an *EphA3* probe to similar retinal sections from *Isl2-EphA3* heterozygotes (G, ki/+) and homozygotes (H, ki/ki) demonstrates an elevated level of *EphA3* mRNA in the latter. In situ reactions for all panels were developed together, and the results were photographed identically. (I) Schematic of *EphA3* expression in wild-type and knockins. Normal mouse retinae (top) exhibit a temporal (t)–nasal (n) RGC gradient of *EphA5* and *EphA6*. *Isl2*-positive RGCs (black cells) and *Isl2*-negative RGCs (gray cells) contribute equally to this gradient. *Isl2-EphA3* heterozygotes (middle) and homozygotes (bottom) have EphA3 expression in *Isl2*+ RGCs superimposed upon the *EphA5/6* gradient; the spikes of superimposed *EphA3* are twice as large in homozygotes relative to heterozygotes. The height of the spikes has been set to reflect the observed *EphA3* mRNA signal relative to the summed endogenous *EphA5/A6* signal, as well as the retinocollicular mapping behavior observed for RGC axons in the knockins (see Figure 5).

Second, *Isl2* is not expressed in the SC. Thus, the induced expression of *EphA3* is limited to the test population of RGCs, and interpretation of experimental results is not complicated by the simultaneous expression in their target. Finally, each experimental analysis in the knockins is internally controlled, since both wild-type and mutant RGCs project to the same SC.

We obtained three ES cell lines with homologous recombination events at the *Isl2* locus (Figures 2A and 2B), and used these to generate knockin mice (see Experimental Procedures). Mice homozygous for the *Isl2-EphA3* allele exhibited no obvious defects in viability or behavior, and were fully fertile. In contrast, homozygous *Isl2* knockouts die at birth (S. L. P. and T. M. J., unpublished data). The *Isl2-EphA3* construct did not perturb expression of *Isl2* (Figures 2E and 2F). This construct encodes a bicistronic mRNA, such that all *Isl2*+ cells should also be EphA3+. This proved to be the case: the RGC layer in homozygous *Isl2-EphA3* neonates exhibited a novel, mosaic pattern of *EphA3* mRNA expression (Figure 2H) that was similar to the pattern of *Isl2* expression (Figures 2E and 2F). This induced *EphA3* expression was not graded across the t-n axis of the retina (Figures 3A and 3D), and did not alter the normal t-n RGC gradient of *EphA5* and *A6* (Figures 3B, 3C, 3E, and 3F). In *EphA3*+ homozygous RGCs, the observed *EphA3* mRNA signal was nearly comparable in intensity to the maximal *EphA5 + A6* mRNA signal seen in the temporal retina

(Figures 3A–3C). RGCs in *Isl2-EphA3* homozygotes expressed a higher level of *EphA3* than heterozygotes (Figures 3G and 3H). Thus, in the RGCs of the *Isl2-EphA3* retina, uniform spikes of EphA3 are superimposed upon the endogenous aggregate gradient of EphA5 and EphA6, as schematized in Figure 3I. A given t-n position in the retina contains RGCs that express a normal level of EphA receptors appropriate for that position; i.e., cells in which the *Isl2-EphA3* allele is silent, which are adjacent to RGCs that express elevated levels of these receptors (Figure 3I).

Anterograde Analysis of the Retinocollicular Projection in *Isl2-EphA3* Mice

RGCs in the nasal region of a wild-type retina are thought to project to the caudal SC because their axons express low levels of the EphA receptors that bind ephrin-A2 and -A5. If this is so, then RGCs at the same nasal location that have acquired elevated levels of EphA receptors should project to more rostral TZs than normal. We tested this idea by performing focal injections of fluorescent anterograde tracers along the retinal t-n axis in wild-type and knockin mice, and then assessing the number and position of the TZs labeled by these retinal injections in the contralateral SC (Figure 4). Injections were performed at P11–P12, when the mouse retinocollicular map is mature. In some mice, we were able to make sequential injections, of DiI (red) and DiAsp (green), into
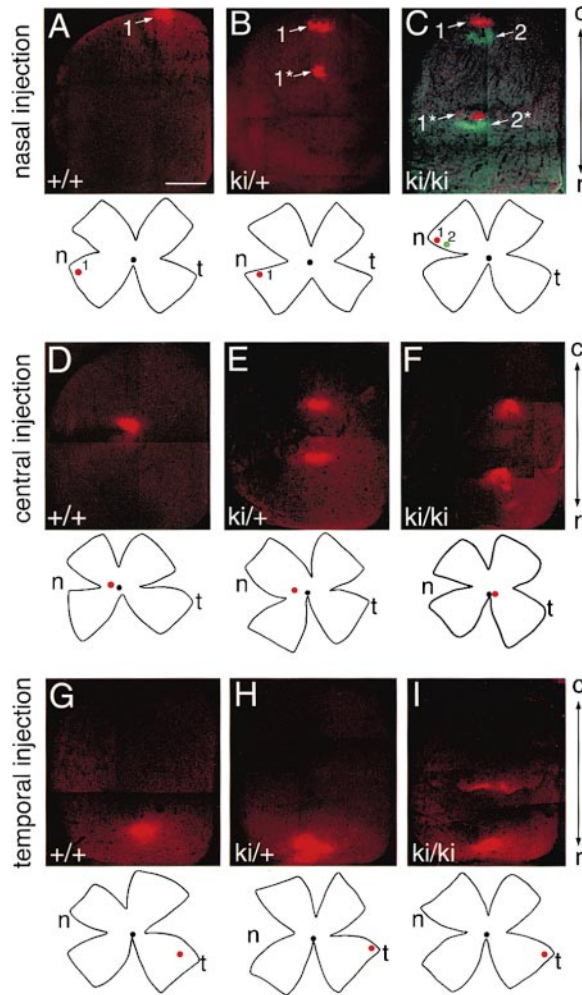
Figure 4. Anterograde Tracing Analysis of the Retinocollicular Projection in *Isl2-EphA3* Mice

(A–C) Injections of DiI (red, 1, for panels A and B), or of DiI (red, 1) and DiAsp (green, 2) sequentially (for panel C), into the nasal retina of wild-type (+/+, A), heterozygous (ki/+, B) and homozygous (ki/ki, C) knockin mice, and visualization of the labeled target fields in the contralateral superior coliculus (SC). In these and all subsequent panels, the position of the injection site(s) (red or green dots) is diagrammed on the retinal flat-mount below the fluorescent montage of the SC. The rostral-caudal axis of the SC (r-c) and the temporal-nasal axis of the retina (t-n) are indicated. In all panels, the medial edge of the SC is to the right. 1 and 2 correspond to SC TZs at the expected positions, while 1* and 2* correspond to rostrally shifted zones.
(D–F) Single injections of DiI into the central retina of wild-type (+/+, D), heterozygous (ki/+, E), and homozygous (ki/ki, F) knockin mice, respectively, and visualization of the labeled TZs in the SC.
(G–I) Single injections of DiI into the temporal retina of wild-type (+/+, G), heterozygous (ki/+, H) and homozygous (ki/ki, I) knockin mice, respectively, and visualization of the labeled TZs in the SC. Scale bar = 500 μm.

the RGC layer of the same retina. In a normal retina, (Figure 4A), a single nasal DiI injection yielded a single DiI-labeled TZ in the caudal SC (1, arrowed), as expected. In contrast, a simliar nasal injection in *Isl2-EphA3* heterozygotes (Figure 4B) always yielded two termination zones, one at the anticipated caudal position (1 in Figure 4B), and a second more rostral zone

(1*). These results indicate that the retinocollicular map of the *Isl2-EphA3* heterozygotes is well ordered, but that a given field of RGCs projects to two distinct TZs separated along the r-c axis.

Injections into the nasal retina of *Isl2-EphA3* homozygotes—paired sequential injections of DiI and DiAsp are illustrated in Figure 4C—also always yielded two TZs in the SC. One of these was located at the anticipated caudal position (red TZ1 for DiI and green TZ2 for DiAsp), and a second ectopic TZ was again located at a more rostral site (red TZ1* for DiI and green TZ2* for DiAsp). However, the disparity between the relative r-c positions of these two TZs was much greater than the TZ separation seen in the heterozygotes (compare Figures 4B and 4C). Thus, a 2-fold increase in gene dosage of the *Isl2-EphA3* allele resulted in an increase in the rostral-ward shift of "ectopic" TZs. On average, this shift was itself ~2-fold: nasal retinal injections in mice with one knockin allele yielded an average rostral-ward shift of 18.0% ± 1.2% (n = 8) of the r-c axis in the SC, while the same shift in *Isl2-EphA3* homozygotes was 38.9% ± 4.8% (n = 8).

We carried out similar injections into the central and temporal retinae of wild-type and *Isl2-EphA3* knockins at P11–P12 (Figures 4D–4F and 4G–4H). Single injections performed in the central retina again always yielded two rather than one TZ in the knockins. However, the relative r-c axial position of *both* TZs was increasingly shifted relative to wild-type, particularly in the homozygotes. The more caudal SC termination zone was displaced caudally, relative to the position seen in wild-type, whereas the more rostral TZ was shifted rostrally (compare Figures 4D and 4E). These displacements were again more pronounced in *Isl2-EphA3* homozygotes than in heterozygotes (compare Figures 4E and 4F). Because of this, it was difficult to characterize the location of one TZ as "normal" and the other as "ectopic."

Anterograde injections targeted to extreme temporal retina revealed a striking difference in the number and position of SC TZs in heterozygous versus homozygous knockins. In *Isl2-EphA3* heterozygotes (ki/+), injections in the most temporal 15% of the retina *never* (n = 12) yielded two distinct TZs in the SC; a typical example, similar to the TZ seen for an equivalent injection in wild-type, is shown in Figure 4H. In marked contrast, we *always* (n = 9) observed two TZs following injections into extreme temporal retinae from *Isl2-EphA3* homozygotes (ki/ki in Figure 4I). Note that in the latter case, the apparently "ectopic" TZ is shifted caudally relative to the wild-type position, rather than rostrally as seen for the nasal injections, and occupies a site near the middle of the SC. These observations led us to determine the retinal-collicular topographic mapping function across the full t-n extent of the retina for wild-type and *Isl2-EphA3* hetero- and homozygous mice.

The Retinocollicular Mapping Function in *Isl2-EphA3* Mice

We collected data from single injection points across the t-n axis in 49 retinae (from 49 mice), and then plotted the r-c axial location of the center of the observed collicular TZs relative to the t-n position of each injection site. The retinocollicular mapping functions thereby generated (Figure 5) proved to be particularly informative.
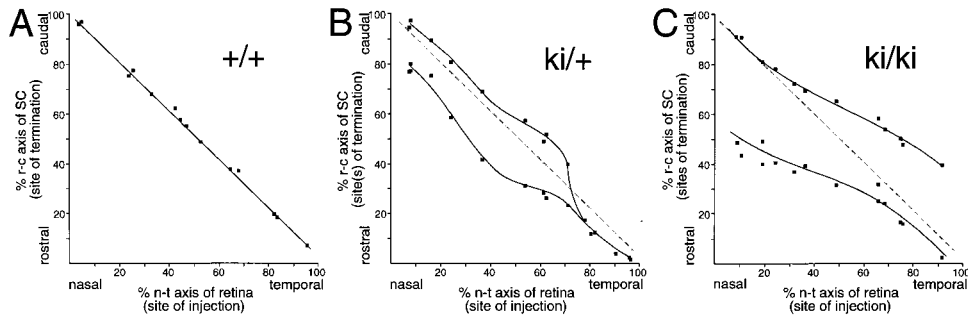
Figure 5. The Retinocollicular Mapping Functions in *Isl2-EphA3* Mice

The r-c position of the centers of SC TZs produced from DiI and DiAsp injections, performed (as in Figure 4) across the full temporal-nasal extent of the retinae of wild-type and knockin mice, were plotted against the temporal-nasal axial location of the retinal injection site. Data plotted represent the subset of injections performed for which complete tissue reconstructions of both the injected retina and its associated SC were carried out. (A) The wild-type function is described by a single linear curve. (Fourteen experiments plotted.) (B) The heterozygous (ki/+) function is described by two curves along the nasal-most 70% of the retinal t-n axis, which collapse to a single curve along the temporal-most 25% of this axis. The separation between the two curves at the nasal end of the retinal axis averages 17% of the r-c axis of the SC. The position of the wild-type curve of (A) is indicated by the dashed gray line. (Fifteen experiments plotted.) (C) The homozygous (ki/ki) function is described by two, approximately linear curves throughout the entirety of the retinal axis. The separation between these two curves averages 38% of the r-c axis of the SC. The position of the wild-type curve of (A) is indicated by the dashed gray line. (Twelve experiments plotted.)

Whereas the wild-type function defines a linear curve that runs from 0%–100% of the collicular r-c axis (extreme rostral to extreme caudal) as the retinal injection position moves from extreme nasal to extreme temporal (Figure 5A), the *Isl2-EphA3* homozygote map consists of points that define two distinct curves (Figure 5C). These curves are also nearly linear, but are separated from each other by approximately 40% of the r-c axis at the extreme nasal end of the retinal axis, and somewhat less so at the temporal end of this axis (Figure 5C). In this map, every point on the retinal (x) axis maps to at least two points along the SC (y) axis. Approximately 10% (2/22) of secondary TZs in the homozygotes are split into two zones that occupy slightly different rostral-caudal and/or medial-lateral positions in the SC. (The points at 20% of the retinal t-n axis in Figure 5C are an example of an r-c split.) These infrequent split TZs are most probably an artifact of the injection procedure, which may occasionally kill RGCs or sever their axons at the center of the injection site; however, we cannot rule out the possibility that they reflect a weak contribution of EphA signaling to medial-lateral mapping (Feldheim et al., 2000). The two curves of the homozygous knockins, both of which are shallower in slope than the single wild-type curve, suggest the formation of separate and independent retinocollicular maps. These maps roughly subdivide the rostral and caudal halves of the SC, but overlap from ~40%–60% of the collicular r-c axis (Figure 5C). Neither curve corresponds to the wild-type function (dashed gray line in Figure 5C).

The *Isl2-EphA3* heterozygote mapping function (Figure 5B) is in two respects intermediate between the wild-type and homozygote functions. Like the homozygote map, the heterozygote function yields two approximately linear curves in the nasal-most 70% of the retinal t-n axis. However, these two curves converge into a single curve at ~75% of the t-n axis (Figure 5B). All retinal injections performed from 0%–60% of the t-n axis (n = 14) yielded double TZs in the SC, ~18% of which exhibited secondary TZs that were split along the

collicular m-l axis; however, *none* of those performed from 80%–100% of the retinal t-n axis (n = 12; 6 plotted in Figure 5B) yielded more than a single TZ. These results are suggestive of a bifurcated retinocollicular map in the caudal-most 60% of the SC, which collapses to a single coherent map in the rostral-most 20% of the SC. Both the observed covergence at the rostral end of the heterozygote map, and its absence in the homozygotes, are consistent with the relative difference in the ratio of EphA3 to EphA5/6 seen in nasal versus temporal retina (see Discussion).

The second feature of the *Isl2-EphA3* heterozygote mapping function that is intermediate between the wild-type and homozygous functions is the r-c displacement observed between the two curves generated from injections into the nasal-most 60% of the retina. The separation between the two curves in the nasal portion of the homozygote mapping function is approximately twice that of the heterozygote function (Figures 5B and 5C), consistent with the ~2-fold difference in *EphA3* expression observed in homozygotes versus heterozygotes (Figures 3G and 3H). The reduction in curve separation in the heterozygotes translates into a correspondingly greater overlap in the collicular areas that are covered by the two maps.

Retrograde Analysis of Retinocollicular Projections in *Isl2-EphA3* Mice

The mapping functions of Figure 5 predict both the position and number of retinal RGC fields that should be back-labeled by focal injection of retrograde axonal tracers into the SC. For example, injections into either the caudal or the rostral SC of *Isl2-EphA3* homozygotes should retrogradely label a single projection field of RGC neurons, in the nasal and temporal retina, respectively; whereas an injection into the central SC, where the upper and lower curves overlap, should label two RGC fields, whose positions should correspond to the x axis intercepts of these curves.

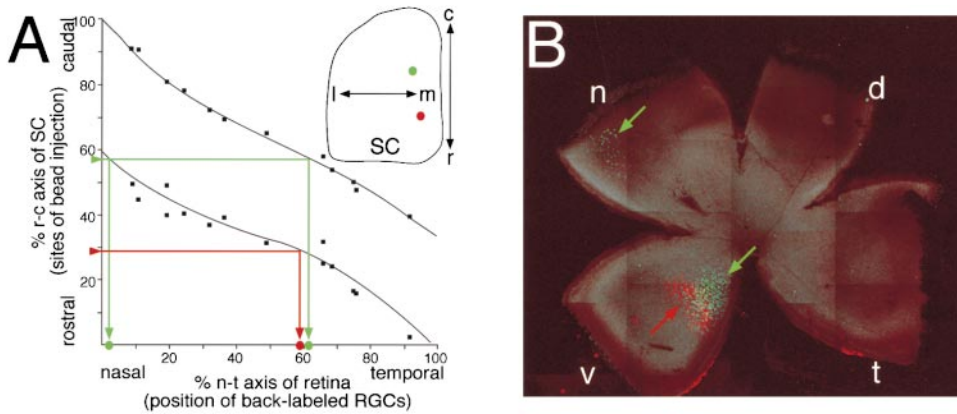We tested these predictions by retrogradely labeling

Figure 6. Predictions and Results from Retrograde Tracing Analysis of the Retinocollicular Projection in Homozygous *Isl2-EphA3* Mice

(A) From the mapping function of Figure 5C are shown the predicted positions of RGC fields along the t-n axis of the retina (dots on x axis) that should be labeled by injection of fluorescent latex beads into the SC of *Isl2-EphA3* homozygotes at 57% of the collicular r-c axis (green arrow, lines, and dots) and at 28% of the r-c axis (red arrow, lines, and dot). The single green bead injection at 57% of the collicular r-c axis intersects both upper and lower curves, and is therefore predicted to yield two retrogradely labeled RGC fields in the retina, one at ∼60% of the t-n axis and a second in extreme nasal retina. The single injection of red beads intersects only the lower curve, and is therefore predicted to yield a single retrogradely labeled RGC field at ∼60% of the t-n axis, immediately nasal to the green RGC field at this position. The positions of the red and green bead injections for this experiment, along both the rostral-caudal (r-c) and medial-lateral (m-l) axes of the SC, are indicated in the inset diagram. (B) Flat-mount montage of the contralateral retina connected to the SC injected in (A). The temporal-nasal (t-n) and dorsal-ventral (d-v) axes of this retina are indicated. Two green RGC fields are labeled—a major one at ∼60% of the retinal t-n axis, and a minor one in extreme nasal retina. A single red RGC field is labeled. This field is at ∼60% of the retinal t-n axis, and is immediately nasal to and partially overlapping with the green RGC field at this position. The red retrogradely labeled RGC field is slightly ventral to the green field, which is consistent with the fact that the red bead injection site in the SC is slightly medial to the green site (Figure 6A inset).

RGCs with focal injections of fluorescent (red- or green-labeled) latex beads (Katz et al., 1984) into various positions within the SC (see Experimental Procedures). The methodology and results of a typical experiment are illustrated in Figure 6, where we injected red beads into the rostral SC of an *Isl2-EphA3* homozygote, at a site centered at 28% of the r-c axis. This site is predicted to intercept only the lower curve of Figure 5C and thus to yield a single retrogradely labeled RGC field at ∼58% of the retinal t-n axis. Into the same SC, we also injected green beads at ∼57% of the r-c axis, a site that is predicted to intercept both the upper and lower curves of Figure 5C, and thus to yield two retrogradely labeled RGC fields, at ∼3% and ∼60% of the retinal t-n axis. These two predictions are diagrammed in Figure 6A, the inset of which displays a flat-mount diagram of the injected SC on which the actual positions of the red and green injection sites are indicated. The results of this double-injection experiment are shown in the retinal flat-mount montage of Figure 6B. They conform well to the predictions made from the homozygous anterograde mapping function. First, there is a single back-labeled red RGC field in the retina, but two back-labeled green RGC fields; second, the positions of the red and green fields along the t-n axis are as predicted by the curve intercepts (Figure 6A); and third, the temporal-most green field is nearly coincident with, but immediately temporal to, the red field (Figure 6A). Note also that the green retinal RGC field is just dorsal to the red field (Figure 6B), in keeping with the fact that the green bead injection site in the SC is positioned immediately lateral to the red site (inset, Figure 6A).

We carried out a series of similar single-color retrograde axonal tracings across the full r-c extent of the SC in both wild-type and *Isl2-EphA3* homozygous mice. Representative results from injections into caudal, central, and rostral SC are illustrated in Figure 7. Injections into the caudal-most 20% of the SC in either wild-type or *Isl2-EphA3* homozygotes (Figures 7A and 7B) back labeled a single RGC field in the contralateral retina, and the t-n axial positions of these fields were not significantly different from each other, as predicted by the x axis intercepts of the curves in Figures 5A and 5C, respectively. Injection of beads into the central SC of wild-type mice back-labeled a single RGC field in the center of the t-n axis of the retina (Figure 7C), but a similar injection in *Isl2-EphA3* homozygotes back-labeled two separate RGC fields, which are now located at opposite ends of the retinal t-n axis (Figure 7D). Again, the number and retinal t-n position of these fields are predicted by the x axis intercepts of the curves in Figures 5A and 5C. Finally, injection into the rostral SC at ∼30% of the r-c axis labeled a single field in the temporal retina of wild-type mice, at ∼70% of the t-n axis (Figure 7E); and a similarly positioned collicular injection in *Isl2-EphA3* homozygotes also labeled a single retinal RGC field, but this field is now positioned near the center of the t-n axis (Figure 7F).

The most straightforward interpretation of the mapping functions displayed in Figures 5B and 5C is that the more caudal (upper) SC curves correspond to RGCs whose axons are EphA3^{−}, while the more rostral curves correspond to EphA3^{+} RGCs. We tested this interpretation by performing focal injections of fluorescent latex beads near the r-c midpoint of the *Isl2-EphA3* homozygous SC, at 45% of the collicular r-c axis (Figure 8A). This axial position intersects both the upper and lower curves of Figure 5C, at ∼20% and ∼80% of the retinal
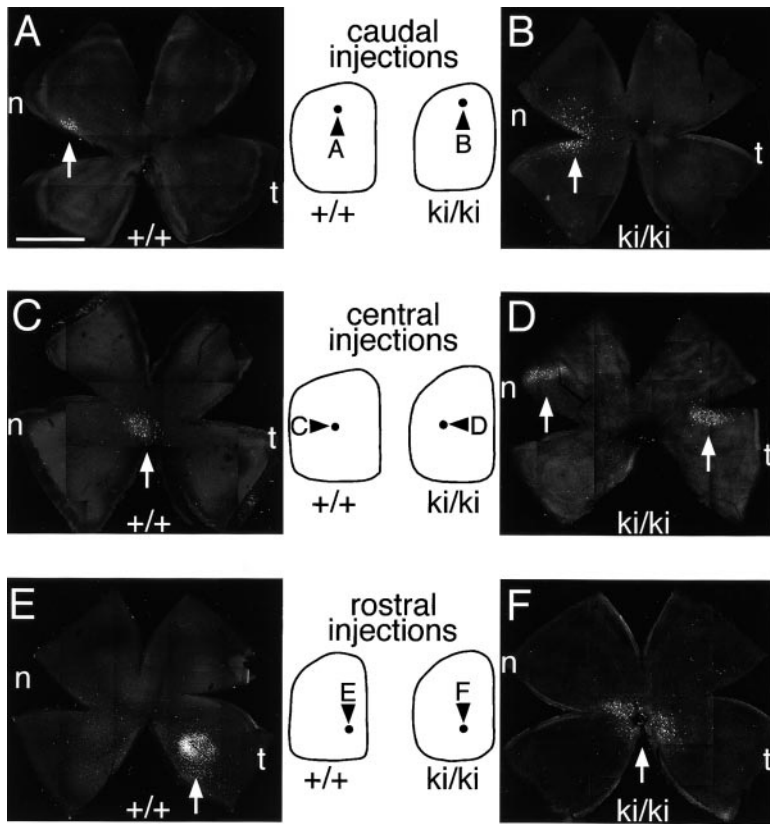
Figure 7. Retrograde Axon Tracing of the Retinocollicular Projection across the Rostral–Caudal Axis of the SC in Wild-Type and *Isl2-EphA3* Homozygotes

Single latex bead injections were performed in the SC at similar caudal (A and B), central (C and D), and rostral (E and F) positions in wild-type (+/+, A, C, and E) and *Isl2-EphA3* homozygous mice (ki/ki, B, D, and F). For each panel, the position of the SC injection site is indicated in the central diagram (arrowed dots), and the position(s) of the RGC field(s) retrogradely labeled by each single injection (white arrows) is displayed in the adjacent retinal flat-mount montage. The orientation of the temporal-nasal (t-n) axis of each retinal montage is indicated. The medial edge of the SC is to the right. Scale bar = 1 mm.

t-n axis, respectively; and as expected, this single injection back-labeled two RGC fields at these positions (Figure 8B). We sectioned blocks of fixed retinal tissue containing the fluorescent beads in each of these fields, and performed digoxygenin-based in situ hybridization for *EphA3* mRNA on these sections. Our results predict that the temporal back-labeled RGC field of Figure 8B (at ~80% of the t-n axis) should be composed predominantly of cells that do not express knocked-in *EphA3*, since the position of this field corresponds to the intercept with the upper curve of Figure 5C. Similarly, the nasal RGC field is predicted to be composed predominantly of EphA3$^+$ neurons. Consistent with these predictions, we found that bead-labeled RGCs expressing the highest levels of *EphA3* mRNA were located exclusively in the nasal projection field (Figure 8C, upper panel). (186 bead-labeled nasal RGCs were scored.) Similarly, bead-labeled RGCs in the temporal field (248 bead-labeled RGCs scored) were largely devoid of *EphA3* (Figure 8C, lower panel).

Discussion

Our data provide quantitative in vivo evidence for the hypothesis that the graded expression of EphA receptors by retinal neurons regulates topographic mapping of the temporal-nasal axis of the retina onto the rostral-caudal axis of the superior colliculus. They support a model of retinocollicular mapping in which the net level of EphA receptors expressed on an RGC axon, and the concentration of collicular ephrin-A ligands to which these receptors are exposed, together specify the r-c

position at which RGC neurons establish their terminal arbors. However, they further indicate that the level of EphA signaling is not an absolute or fixed determinant of retinocollicular mapping, but that it is instead interpreted by developing RGCs in the context of competition with their neighbors for synaptic targets, axon branching pathways, or other features of the neonatal SC that are present in limiting amounts.

Relativity and Competition in EphA Signaling

The retinocollicular projection in the *Isl2-EphA3* homozygotes has several informative features. First, there are two maps rather than one, and *neither* map is normal. Second, the axons of EphA3$^-$ (wild-type) RGCs appear to be pushed from the rostral SC by their EphA3$^+$ neighbors. Third, even extreme temporal EphA3$^+$ RGCs, which express much higher EphA levels than any RGCs in a wild-type retina, still map to the SC. Fourth, the two maps together fill the entire SC, with no evident gaps. Fifth, the relative EphA level of an individual RGC axon, compared to all other RGC axons, appears to provide positional information: axons with the highest EphA level assume the most rostral collicular site. Sixth, RGCs in opposite parts of the retina, but with the same EphA level, project to the same TZ in the SC. Correspondingly, adjacent RGCs in the retina send axons to different TZs in the SC, if they express EphA receptors at different levels. And seventh, RGC axons appear to mutually discriminate degrees of EphA signaling among themselves: a temporal axon that is normally targeted to a rostral site will project more caudally if it encounters RGC axons with higher EphA levels than itself.
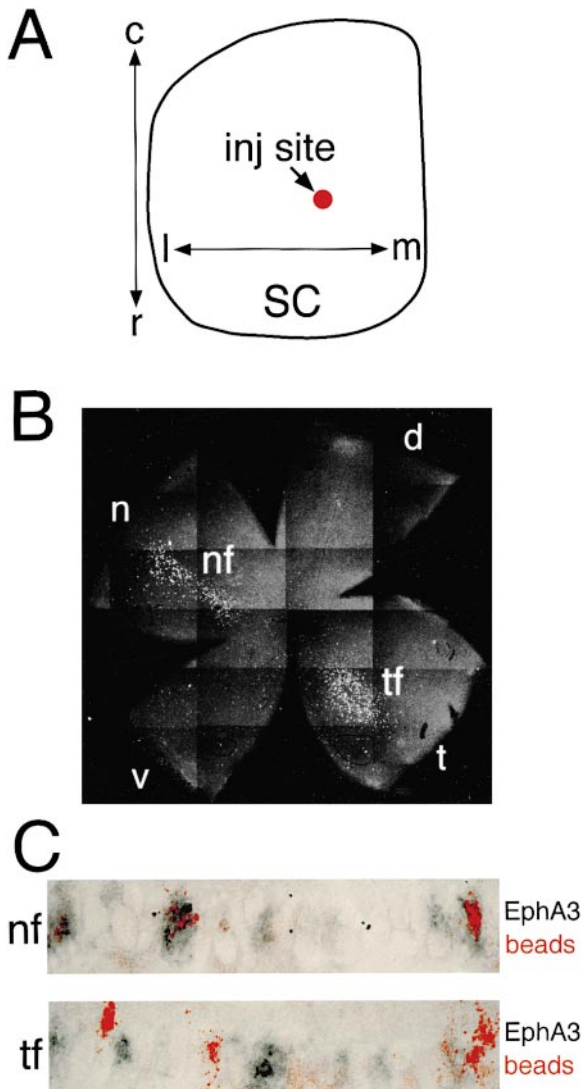
Figure 8. *EphA3* Expression in the Retrogradely Labeled RGC Fields of *Isl2-EphA3* Homozygotes

(A) Red fluorescent latex beads were injected as retrograde axonal tracers into the SC of an *Isl2-EphA3* homozygote, at ~45% of the collicular rostral-caudal (r-c) axis. The location of the injection site (arrowed red dot) with respect to both the r-c and medial-lateral (m-l) axes of the SC is indicated. (B) Montage of a flat-mount of the retina connected to the SC injected in (A). A nasal RGC projection field (nf) and a temporal field (tf), which occupy temporal-nasal (t-n) axial positions predicted by the anterograde mapping function of Figure 5C, are visualized. The dorsal-ventral (d-v) axis of the retina is also indicated. (C) Sections through the RGC layer of either the nasal field (nf) or the temporal field (tf) of the retinal flat-mount of (B) were hybridized with a digoxygenin-labeled *EphA3* probe to visualize *EphA3* mRNA (black signal) in cells either labeled or unlabeled by retrogradely transported red beads. Note that for the nasal field (top panel), *EphA3+* cells are also bead-labeled, and bead-labeled cells are also *EphA3+*; but for temporal field (bottom panel), *EphA3+* cells are not bead-labeled, and bead-labeled cells are not *EphA3+*.

Each of these features of RGC mapping in the knockins are best explained if EphA signaling is modulated by competition between RGC axons. One possible outcome of our experiments was that the map formed by

the EphA3− RGCs in the knockins would cover the entirety of the r-c axis of the SC, as it does in wild-type mice, and that only the map formed by EphA3+ axons would be compressed rostrally as a result of their higher level of EphA receptors (see Figure 5C). However, we found that the two maps of the homozygous knockins are largely nonoverlapping (Figure 5C), with the r-c position at which EphA3− temporal axons arborize approximating that of EphA3+ nasal axons. This implies that most EphA3+ axons are more strongly repelled by ephrin-A ligands than are EphA3− temporal axons, and demonstrates that the axonal responses mediated by the normally high level of endogenous EphA receptors in temporal RGCs are not saturating. Moreover, our results suggest that the absolute level of EphA signaling is not by itself determinative with respect to the final r-c position of TZs, since EphA3− temporal axons terminate in mid-SC in *Isl2-EphA3* homozygotes, a position that is inappropriate for the level of EphA receptors that they express. The mapping of the EphA3+ and EphA3− RGCs in the homozygous knockins suggests a continuum in the overall level of EphA signaling; that is, within each map, the level of EphA signaling exhibits a decreasing t-n gradient, and both the signaling level and mapping of EphA3+ nasal RGCs approximates that of EphA3− temporal RGCs.

An additional feature of retinocollicular mapping in the knockins that argues for relative but not absolute EphA signaling is the observed difference in the mapping of EphA3+ and EphA3− temporal axons between the homozygous and heterozygous mice. The EphA5/6 receptor gradient runs from high temporal to low nasal, and as a consequence there is a greater relative disparity in summed EphA receptor levels between EphA3+ and EphA3− RGCs in the nasal as opposed to the temporal retina of *Isl2-EphA3* heterozygotes, given a fixed level of superimposed EphA3 across the t-n axis. The data of Figure 5B suggest that the level of superimposed EphA3 expression in the extreme temporal retinae of the heterozygotes is sufficiently modest relative to the high endogenous EphA5/6 levels such that there is little or no discrimination between EphA3+ RGCs, which express EphA3 in addition to EphA5 and A6, and the EphA3− cells that express only the endogenous receptors.

Coordinated electrical activity among neighboring RGCs normally plays a significant role in establishing orderly visual projections (Katz and Shatz, 1996), including the refinement of the rodent retinocollicular projection (Simon et al., 1992). Although we cannot exclude the possibility that EphA receptors influence the development of intraretinal connections, such that EphA3+ and EphA3− RGCs become electrically independent populations in the knockins, our observations that (a) EphA-equivalent RGCs from completely different parts of the retina map to the same collicular TZ, and (b) EphA3+ and EphA3− RGCs at the same retinal site map to disparate sites in the SC, together argue that EphA receptor levels determine targeting, not neighbor relationships in the retina.

Models for Modulation of EphA Action
The molecular and cellular basis for the caudal "compression" of EphA3− RGCs in the homozygous knockins

is at present unclear. One possibility is that the EphA3^{+} and EphA3^{−} populations interact competitively for limiting "collicular space" (reviewed in Goodhill and Richards, 1999), and that the EphA3^{+} population excludes the EphA3^{−} population from limiting branching pathways or synaptic target sites in the rostral SC, which are preferentially occupied by EphA3^{+} axons. Such a possibility is in keeping with earlier "systems matching" models for retinotectal innervation (Gaze and Keating, 1972; Goodhill and Richards, 1999). Axon–axon competitive interactions, for example those based on activity-dependent mechanisms, may also contribute to the caudalward displacement of the EphA3^{−} RGCs.

Not exclusive with these competitive interactions is the possibility that the caudal compression of the EphA3^{−} RGC map in the homozygous knockins could result from an alteration in the smoothly graded profile of ephrin-A expression along the r-c axis of the SC. EphA receptors and ephrin-A ligands are normally expressed in countergradients by wild-type RGCs (Marcus et al., 1996). EphA receptors are also normally phosphorylated at a higher level in nasal as opposed to temporal retina (Connor et al., 1998; Hornberger et al., 1999), and the countergradient of retinal ephrin-As has been hypothesized to enhance the gradient of EphA receptor signaling by preferentially reducing the pool of functional EphA receptors (e.g., EphA4) in the nasal retina (Hornberger et al., 1999). However, since ephrin-A ligands are also present on RGC axons, with the highest levels on nasal axons (Marcus et al., 1996; Monschau et al., 1997; Connor et al., 1998; Hornberger et al., 1999), these retinal ligands may in addition contribute to the development of topographic order in the SC (McLaughlin and O'Leary, 1999). As wild-type nasal axons normally arborize and increase their surface area in the caudal SC during map development, the net level of ephrin-A repellent activity may also increase preferentially in the caudal SC, and the establishment of retinocollicular topography may thus depend upon the summed repellent activity resulting from ephrin-A expression by SC cells and by RGC axons. If this possibility holds, then the aberrant, compressed mapping of EphA3^{+} axons in the homozygous knockins may alter the normal smoothly increasing gradient of collicular ephrin-As, and thereby generate an abnormally steep gradient of ephrin-A repellent activity in the rostral SC. This abnormal gradient would exhibit an abrupt decline, to a lower than normal level, in the mid-SC, i.e., at the caudal limit of the EphA3^{+} map. In response to this change in the overall ephrin-A expression profile along the collicular r-c axis, EphA3^{−} temporal axons would arborize more caudally than normal.

EphA Signaling in Development

Graded expression of EphA receptors and their ephrin-A ligands has been observed in several other regions of the developing vertebrate CNS (Feldheim et al., 1998; Mackarehtschian et al., 1999). Gradients of both ephrin-A2 and -A5 have been detected in the developing dorsal and ventral lateral geniculate nuclei (Feldheim et al., 1998), which like the SC are targets of direct retinal innervation. In addition, a graded ephrin-A2-associated repulsion mediated by EphA5 appears to be involved in

establishing topographic order in the hippocamposeptal projection (Gao et al., 1996). Similarly, expression data and in vitro findings suggest that ephrin-A5, acting through EphA3, A4, and A5, may influence the development of topographically ordered thalamocortical projections (Gao et al., 1998; Mackarehtschian et al., 1999). These and related observations indicate that EphA signaling may play a general role in topographic mapping, and that the parameters of EphA receptor action suggested by our findings in the retinocollicular projection may therefore apply to the operation of this important signaling system throughout the developing CNS.

Experimental Procedures

DNA Constructs and Targeting

The *Islet2-EphA3* targeting vector (Figure 2) was prepared by first generating a cassette in which an upstream internal ribosome entry site (from the EMC virus) was ligated at an NcoI site engineered at the start codon of the full-length mouse EphA3 cDNA, which had previously been 3′-terminated with an SV40 polyadenylation signal (a gift of Elena Pasquale). A loxP-flanked pgk-neo cassette for positive selection in ES cells was ligated to the 3′ end of this cassette. The IRES-EphA3-neo segment was flanked by PacI sites, and inserted into the PacI site of a polylinker (5′-SphI-PacI-HindIII-SphI-3′) that had been cloned into an SphI site located within the 3′ untranslated region of the mouse *Islet2* gene (see Figure 2). The *Islet2* genomic clone for this construction was isolated from a 129sv mouse genomic library. The final *Isl2-EphA3* targeting vector was introduced into the mouse *Isl2* genomic locus by homologous recombination in ES cells, which were scored by Southern blot (Figure 2). The floxed neo cassette was not removed. Chimeric mice were prepared by blastocyst injection of these ES cells at the Salk Institute transgenic core facility, and chimeras were then bred with wild-type C57Bl/6 mice to obtain animals heterozygous for the recombined allele.

Expression Analysis

In situ hybridizations with [35]S- or digoxygenin-labeled RNA probes were performed as described (Schaeren-Wiemers and Gerfin-Moser, 1993). Unless otherwise indicated, all tissues were sectioned at 10 μm. For the in situ hybridization reactions of Figure 3, identical length (900 bp) *EphA3*, *A5*, and *A6* RNA probes were synthesized from the 5′ end of each Eph receptor cDNA, hybridized to adjacent retinal sections on the same slides, and developed and photographed under identical conditions.

Axonal Labeling

For anterograde labeling of RGC axons, a small focal injection of DiI, and in some cases an additional injection of DiAsp, was made into the retina at P11–P12, and analyzed 24 hr later (Simon and O'Leary, 1992). The injected retina and contralateral midbrain were prepared as wholemounts and examined with rhodamine (DiI) or fluorescein (DiAsp) optics using a Nikon Microphot fluorescence microscope or a Zeiss LSM 510 confocal microscope. The placement and size of the DiI injections were plotted on drawings of the retinal wholemounts. Montages of labeled retinal axons in the SC were constructed from digital images using NIH image and Adobe Photoshop software.

For retrograde labeling, a small focal injection of fluorescent (red or green) latex microspheres (Katz et al., 1984; Katz and Iarovici, 1990) was made into the SC of P12–P16 mice, as previously described for DiI injections (Simon et al., 1994), and analyzed 24 hr later. The injected SC and the contralateral retina were prepared as wholemounts and examined as described above. The retinal wholemounts were later sectioned sagittally at 10 μm and reexamined. In situ hybridization for *EphA3* mRNA was performed on these sections. Images of latex beads and *EphA3* mRNA signals (detected with a digoxygenin-labeled probe) were scanned together on a Bio-Rad MRC1024 confocal microscope.

Acknowledgments

References

Baier, H., and Bonhoeffer, F. (1992). Axon guidance by gradients of a target-derived component. Science 255, 472–475.

Bastmeyer, M., Ott, H., Leppert, C.A., and Stuermer, C.A. (1995). Fish E587 glycoprotein, a member of the L1 family of cell adhesion molecules, participates in axonal fasciculation and the age-related order of ganglion cell axons in the goldfish retina. J. Cell Biol. 130, 969–976.

Cheng, H.J., and Flanagan, J.G. (1994). Identification and cloning of ELF-1, a developmentally expressed ligand for the Mek4 and Sek receptor tyrosine kinases. Cell 79, 157–168.

Cheng, H.J., Nakamoto, M., Bergemann, A.D., and Flanagan, J.G. (1995). Complementary gradients in expression and binding of ELF-1 and Mek4 in development of the topographic retinotectal projection map. Cell 82, 371–381.

Connor, R.J., Menzel, P., and Pasquale, E.B. (1998). Expression and tyrosine phosphorylation of Eph receptors suggest multiple mechanisms in patterning of the visual system. Dev. Biol. 193, 21–35.

Cox, E.C., Muller, B., and Bonhoeffer, F. (1990). Axonal guidance in the chick visual system: posterior tectal membranes induce collapse of growth cones from the temporal retina. Neuron 4, 31–37.

Davis, S., Gale, N.W., Aldrich, T.H., Maisonpierre, P.C., Lhotak, V., Pawson, T., Goldfarb, M., and Yancopoulos, G.D. (1994). Ligands for EPH-related receptor tyrosine kinases that require membrane attachment or clustering for activity. Science. 266, 816–819.

Drescher, U., Kremoser, C., Handwerker, C., Löschinger, J., Noda, M., and Bonhoeffer, F. (1995). In vitro guidance of retinal ganglion cell axons by RAGS, a 25 kDa tectal protein related to ligands for Eph receptor tyrosine kinases. Cell 82, 359–370.

Eph Nomenclature Committee (1997). Unified nomenclature for Eph family receptors and their ligands, the ephrins. Cell 90, 403–404.

Feldheim, D.A., Vanderhaeghen, P., Hansen, M.J., Frisén, J., Lu, Q., Barbacid, M., and Flanagan, J.G. (1998). Topographic guidance labels in a sensory projection to the forebrain. Neuron 21, 1303–1313.

Feldheim, D.A., Kim, Y.-I, Bergemann, A.D., Frisén, J., Barbacid, M., and Flangan, J.G. (2000) Genetic analysis of ephrin-A2 and ephrin-A5 shows their requirement in multiple aspects of retinocollicular mapp. Neuron 25, 563–574.

Flanagan, J.G., and Vanderhaeghen, P. (1998). The ephrins and Eph receptors in neural development. Annu. Rev. Neurosci. 21, 309–345.

Fraser, S.E., and Hunt, R.K. (1980). Retinotectal specificity: models and experiments in search of a mapping function. Annu. Rev. Neurosci. 3, 319–352.

Frisén, J., Yates, P.A., McLaughlin, T., Friedman, G.C., O'Leary, D. D., and Barbacid, M. (1998). Ephrin-A5 (AL-1/RAGS) is essential for proper retinal axon guidance and topographic mapping in the mammalian visual system. Neuron 20, 235–243.

Gale, N.W., Holland, S.J., Valenzuela, D.M., Flenniken, A., Pan, L., Ryan, T.E., Henkemeyer, M., Strebhardt, K., Hirai, H., Wilkinson, D.G., et al. (1996). Eph receptors and ligands comprise two major specificity subclasses and are reciprocally compartmentalized during embryogenesis. Neuron 17, 9–19.

Gao, P.-P., Zhang, J.-H., Yokoyama, M., Racey, B., Dreyfus, C.F., Black, I.B., et al. (1996). Regulation of topographic projection in the brain—Elf-1 in the hippocamposeptal system. Proc. Natl. Acad. Sci. USA 93, 11161–11166.

Gao, P.-P., Yue, Y., Zhang, J.-H., Cerretti, D.P., Levitt, P., and Zhou, R. (1998). Regulation of thalamic neurite growth by the Eph ligand ephrin-A5: Implications in the development of thalamocortical projections. Proc. Natl. Acad. Sci. USA 95, 5329–5334.

Gaze, R.M., and Keating, M.J. (1972). The visual system and "neuronal specificity." Nature 237, 375–378.

Goodhill, G.J., and Richards, L.J. (1999). Retinotectal maps: molecules, models, and misplaced data. Trends Neurosci. 22, 529–534.

Hornberger, M.R., Dutting, D., Ciossek, T., Yamada, T., Handwerker, C., Lang, S., Weth, F., Huf, J., Wessel, R., Logan, C., et al. (1999). Modulation of EphA receptor function by coexpressed ephrinA ligands on retinal ganglion cell axons. Neuron 22, 731–742.

Jeon, C.J., Strettoi, E., and Masland, R.H. (1998). The major cell populations of the mouse retina. J. Neurosci. 18, 8936–8946.

Kaas, J.H. (1997). Topographic maps are fundamental to sensory processing. Brain Res. Bull. 44, 107–112.

Katz, L.C., Burkhalter, A., and Dreyer, W.J. (1984) Fluorescent latex beads as a retrograde neuronal marker for in vivo and in vitro studies of visual cortex. Nature 310, 498–500.

Katz, L.C., and Iarovici, D.M. (1990). Green fluorescent latex microspheres: a new retrograde tracer. Neuroscience. 34, 511–520.

Katz, L.C., and Shatz, C.J. (1996). Synaptic activity and the construction of cortical circuits. Science 274, 1133–1138.

Mackarehtschian, K., Lau, C.K., Caras, I., and McConnell, S.K. (1999). Regional differences in the developing cerebral cortex revealed by ephrin-A5 expression. Cereb. Cortex. 9, 601–610.

Marcus, R.C., Gale, N.W., Morrison, M.E., Mason, C.A., and Yancopoulos, G.D. (1996). Eph family receptors and their ligands distribute in opposing gradients in the developing mouse retina. Dev. Biol. 180, 786–789.

McLaughlin, T., and O'Leary, D.D.M. (1999). Functional consequences of coincident expression of EphA receptors and ephrin-A ligands. Neuron 22, 636–639.

Miskevich, F., Zhu, Y., Ranscht, B., and Sanes, J.R. (1998). Expression of multiple cadherins and catenins in the chick optic tectum. Mol. Cell. Neurosci. 12, 240–255.

Monschau, B., Kremoser, C., Ohta, K., Tanaka, H., Kaneko, T., Yamada, T., Handwerker, C., Hornberger, M.R., Loschinger, J., Pasquale, E.B., et al. (1997). Shared and distinct functions of RAGS and ELF-1 in guiding retinal axons. EMBO J. 16, 1258–1267.

Nakamoto, M., Cheng, H.-J., Friedman, G.C., McLaughlin, T., Hansen, M.J., Yoon, C., O'Leary, D.D.M., and Flanagan, J.G. (1996). Topographically specific effects of ELF-1 on retinal axon guidance in vitro and retinal axon mapping in vivo. Cell 86, 755–766.

O'Leary, D.D.M., Yates, P.A., and McLaughlin, T. (1999). Molecular development of sensory maps: representing sights and smells in the brain. Cell 96, 255–269.

O'Leary, D.D.M., and Wilkinson, D.G. (1999). Eph receptors and ephrins in neural development. Curr. Opin. Neurobiol. 9, 65–73.

Orioli, D., and Klein, R. (1997). The Eph receptor family: axonal guidance by contact repulsion. Trends Genet. 13, 354–359.

Schaeren-Wiemers, N., and Gerfin-Moser, A. (1993). A single protocol to detect transcripts of various types and expression levels in neural tissue and cultured cells: in situ hybridization using digoxigenin-labelled cRNA probes. Histochemistry 100, 431–440.

Simon, D.K., and O'Leary, D.D.M. (1992). Development of topographic order in the mammalian retinocollicular projection. J. Neurosci. 12, 1212–1232.

Simon, D.K., Prusky, G.T., O'Leary, D.D.M., and Constantine-Paton, M. (1992). N-methyl-D-aspartate receptor antagonists disrupt the formation of a mammalian neural map. Proc. Natl. Acad. Sci. USA 89, 10593–10597.

Simon, D.K., Roskies, A.L., and O'Leary, D.D.M. (1994). Plasticity in the development of topographic order in the mammalian retinocollicular projection. Dev. Biol. 162, 384–393.

Sperry, R.W. (1963). Chemoaffinity in the orderly growth of nerve fiber patterns and connections. Proc. Natl. Acad. Sci. USA 50, 703–710.

Stahl, B., Muller, B., von Boxberg, Y., Cox, E.C., and Bonhoeffer, F. (1990). Biochemical characterization of a putative axonal guidance molecule of the chick visual system. Neuron *5*, 735–743.

Tsuchida, T., Ensini, M., Morton, S.B., Baldassare, M., Edlund, T., Jessell, T.M., and Pfaff, S.L. (1994). Topographic organization of embryonic motor neurons defined by expression of LIM homeobox genes. Cell *79*, 957–970.

Yen, L., Sibley, J.T., and Constantine-Paton, M. (1995). Analysis of synaptic distribution within single retinal axonal arbors after chronic NMDA treatment. J. Neurosci. *15*, 4712–4725.

Zhang, J.H., Cerretti, D.P., Yu, T., Flanagan, J.G., and Zhou, R. (1996). Detection of ligands in regions anatomically connected to neurons expressing the Eph receptor Bsk: potential roles in neuron–target interaction. J. Neurosci. *16*, 7182–7192.

Zhang, L.I., Tao, H.W., Holt, C.E., Harris, W.A., and Poo, M. (1998). A critical window for cooperation and competition among developing retinotectal synapses. Nature *395*, 37–44.